RSC Advances

PAPER

View Article Online
View Journal | View Issue

Cite this: *RSC Adv.*, 2024, **14**, 26596

Electrospun EVOH/AST-120 hybrid nanofiber membranes for removal of indoxyl sulfate from blood†

Makoto Sasaki, [ab] Rieko Hirata,[c] Ayano Konagai[c] and Mitsuhiro Ebara *[ab]

Nanofibers containing activated carbon using poly(ethylene-*co*-vinyl alcohol) (EVOH) were prepared to remove indoxyl sulfate (IS) from the blood. IS is a urinary toxin that is highly toxic and triggers the progression of chronic kidney disease (CKD). Here, nanofibers containing activated carbon (AST-120), which has been used practically as an adsorbent for indole (a precursor of IS), were fabricated *via* electrospinning for the adsorption and removal of IS from the blood. EVOH containing different ethylene ratios was used as the nanofiber material; moreover, the effect of the ethylene ratio on various properties of the nanofibers, such as surface wettability and the IS adsorption rate, was investigated. As a result, EVOH/AST-120 nanofibers comprising EVOH with a low ethylene ratio exhibited faster IS adsorption behavior. This adsorption behavior agreed well with the pseudo-second-order model, suggesting that the diffusion of IS into the nanofibers is the rate-limiting step of the process of adsorption. Furthermore, the nanofibers successfully reduced the IS concentration in the blood under circulating conditions. Therefore, these EVOH/AST-120 nanofibers are expected to greatly improve the prognosis of patients with CKD when used in combination with the current hemodialysis therapy as an IS-adsorbing filter.

Received 20th June 2024
Accepted 10th August 2024

DOI: 10.1039/d4ra04501g

rsc.li/rsc-advances

1 Introduction

Chronic kidney disease (CKD) is a condition in which the filtration function of the kidneys declines, accompanied by the accumulation of uremic toxins, electrolytes, and water in the blood because of a lack of excretion, causing various complications. Approximately 90 substances have been reported as uremic toxins, which are classified into the three following categories: small water-soluble molecules, medium-sized molecules, and protein-bound molecules.[1] During hemodialysis, which is the main treatment for CKD, uremic toxins are removed *via* their transfer from the blood to the dialysate using the principles of diffusion and filtration. In this process, uremic toxins are transferred through holes located on the surface of the dialysis membrane, which have a diameter of a few nanometers.[2] Thus, small water-soluble molecules, such as urea, can be efficiently removed during hemodialysis, whereas medium-sized molecules, such as β_2-microglobulin and protein-bound molecules (*e.g.*, indoxyl sulfate (IS) and *p*-cresyl sulfate) are removed less efficiently.[3,4] Among these uremic toxins, IS is highly toxic, as it triggers the progression of CKD by causing fibrosis in the kidneys[5,6] and increases the risk of cardiovascular disease,[7,8] which render its removal highly necessary. However, the clearance of IS *via* hemodialysis is very low, around 25–30 mL min^{-1}, which is only 10% of the clearance of urea.[9]

AST-120 is a form of activated carbon that is administered as an oral adsorbent to patients in the conservative phase of CKD. It is responsible for adsorbing uremic toxins in the gastrointestinal tract, thereby suppressing their accumulation in the body.[10–12] The use of AST-120 is mainly intended to delay the onset of hemodialysis; therefore, it is nsot suitable for the treatment of patients with CKD. Therefore, the removal of IS directly from the blood is expected to arrest the progression of CKD and reduce the risk of cardiovascular disease and osteoporosis in patients undergoing hemodialysis.

To use AST-120 for the removal of IS from the blood, it is necessary to prevent its leakage into the bloodstream and avoid direct contact with the blood. Therefore, we need to create new materials containing activated carbon. We developed a method for incorporating AST-120 into nanofibers prepared using polymers. Previously, we reported the preparation of several nanofibers for the removal of uremic toxins using electrospinning,[13–15] and we expected that this technique could be applied in the present context. The electrospinning method is the most common nanofiber-production technique and uses

[a]*Research Center for Macromolecules and Biomaterials, National Institute for Materials Science (NIMS), 1-1 Namiki, Tsukuba, Ibaraki, 305-0044, Japan. E-mail: EBARA.Mitsuhiro@nims.go.jp*

[b]*Graduate School of Pure and Applied Sciences, University of Tsukuba, 1-1-1 Tennodai, Tsukuba, Ibaraki, 305-8577, Japan*

[c]*Research and Development Division, Kureha Corporation, 16 Ochiai, Nishiki-machi, Iwaki, Fukushima, 974-8686, Japan*

† Electronic supplementary information (ESI) available. See DOI: https://doi.org/10.1039/d4ra04501g

electrostatic repulsion when a high voltage is applied to a polymer solution.[16–22] In covering the surface of activated carbon with polymers by electrospinning, it is necessary to carefully consider which polymers to use. Although a high adsorption rate of IS is desirable for the use in hemodialysis, the adsorption rate is expected to decrease when the surface of the activated carbon is covered with a polymer. We hypothesized that the use of hydrophilic polymers might help maintain high adsorption rate: because indoxyl sulfate is a hydrophilic molecule and would be expected to diffuse more quickly into the hydrophilic polymer layer. To demonstrate this hypothesis, poly(ethylene-*co*-vinyl alcohol) (EVOH) was used here as the nanofiber material because the physical properties of EVOH such as hydrophilicity vary greatly according to the copolymerization ratio of the ethylene units to the vinyl alcohol units (ethylene ratio).[23,24] EVOH is also a highly blood-compatible material with a proven track record of practical use as a material for the production of hemodialysis membranes.[25] The purpose of the present study was to fabricate nanofibers containing AST-120 and to evaluate the effect of the ethylene ratio of EVOH on its IS adsorption performance and hemocompatibility.

2 Experimental

2.1 Materials

Crushed AST-120 was kindly supplied by Kureha Corporation (Tokyo, Japan). The EVOH copolymer Soarnol V2504RB with 25 mol% ethylene was purchased from Mitsubishi Chemical Corporation (Tokyo, Japan). The EVOH copolymer E105A was purchased from Kuraray Co., Ltd (Tokyo, Japan). 1,1,1,3,3,3-Hexafluoro-2-propanol was purchased from Tokyo Chemical Industry Co., Ltd (Tokyo, Japan). Dulbecco's phosphate-buffered saline and human serum albumin were purchased from Nacalai Tesque Inc. (Kyoto, Japan). 3-Indoxyl sulfate potassium salt was purchased from Carbosynth (Berkshire, UK), and the IS assay kit was purchased from Nipro Corporation (Osaka, Japan). Moreover, 25% glutaraldehyde and ethanol (super dehydrated) were purchased from Fujifilm Wako Pure Chemical Corporation (Osaka, Japan). Porcine blood was purchased from Tokyo Shibaura Zoki (Tokyo, Japan) as an animal specimen for medical device research. Whole porcine blood was collected during the slaughter and dissection of pigs for meat. To prevent coagulation, a 3.24% sodium citrate solution was added to the porcine blood and transported to the laboratory under refrigeration. Finally, the Micro BCA™ Protein Assay Kit was purchased from Thermo Fisher Scientific K.K. (Tokyo, Japan).

2.2 Preparation of the EVOH/AST-120 nanofibers *via* electrospinning

EVOH with an ethylene ratio of 25 mol% (EVOH25) and 44 mol% (EVOH44) was dissolved in 1,1,1,3,3,3-hexafluoro-2-propanol at a concentration of 4 wt%. The dissolution was performed by applying ultrasonic waves overnight. Crushed AST-120 was fed into a 4 wt% EVOH solution at concentrations of 10, 20, and 30 wt% with respect to the polymer, then dispersed by applying ultrasonic waves for 1 min. Subsequently, electrospinning was performed using the following conditions: applied voltage, 25 kV; feed rate, 1.0 mL h^{-1}; distance between the collectors, 15 cm; and needle size, 22G; followed by collection on aluminum covering the collectors.

2.3 Observation of the EVOH/AST-120 nanofibers

The obtained nanofiber mesh was coated with a platinum sputter and observed using a field emission scanning electron microscope (Hitachi SU8230). The diameters of the fibers were measured from the captured FE-SEM images using the ImageJ software. Elemental mapping of the nanofiber surface was performed *via* energy-dispersive X-ray spectroscopy (EDX) using FE-SEM.

2.4 Physical properties of the EVOH/AST-120 nanofibers

The content of AST-120 in the nanofibers was assessed using a thermogravimetric differential thermal analysis (TG-DTA, Seiko Instruments TG/DTA6200). The content was calculated from the residual mass of 5 mg of fiber mesh when the temperature was increased from 25 °C to 500 °C at a rate of 10 °C min^{-1} and held at 500 °C for 30 min.

The mechanical properties of the nanofibers were evaluated by examining their behavior when subjected to a tensile test (Shimadzu EZ-SX). Each nanofiber was cut into 1–3 cm rectangles, and the stress and strain were measured while applying the load in the longitudinal direction at 10 mm min^{-1}.

The surface wettability of the EVOH/AST-120 nanofibers was evaluated by measuring the contact angle in air using an automatic contact angle meter (Kyowa Interface Science DM-700). A 1 μL drop of water was deposited onto nanofibers that were fixed on a glass slide, and the drop was photographed 3 s later, to measure the contact angle.

Fourier transform infrared spectroscopy (FT-IR) measurements were performed for AST-120 powder and fabricated nanofibers in absorbance mode (Shimadzu IRAffinity-1S). The spectra were measured from 500 cm^{-1} to 4000 cm^{-1} with 64 scans and a resolution of 4 cm^{-1}.

2.5 Evaluation of human serum albumin (HSA) adsorption onto the EVOH/AST-120 nanofibers

Human serum albumin (HSA) adsorption was evaluated, to assess hemocompatibility. The samples were immersed in PBS for 1 h, then in 1 mg mL^{-1} HSA solution, and finally shaken at 37 °C for 1 h. After washing the samples five times with PBS, to remove the excess of HSA, the samples were immersed in a 5% SDS solution (solvent: 0.1 N NaOH) and shaken at 37 °C for 1 h, to detach the adsorbed HSA. Finally, the concentration of HSA in the supernatant was measured using the BCA method, to calculate the amount of HSA that was adsorbed onto the sample.

2.6 Evaluation of platelet adhesion to the EVOH/AST-120 nanofibers

Platelet-rich plasma (PRP) was obtained *via* the centrifugation of porcine blood. EVOH nanofibers and EVOH/AST-120 nanofibers

were immersed in PBS and allowed to stand at room temperature for 3 h. Each sample was then immersed in PRP; after 2 h at 37 °C, each sample was washed twice with PBS, to remove the excess of platelets. To fix the platelets that had adhered to the surface of the sample, each sample was immersed in a 2.5% glutaraldehyde solution and allowed to stand for 2 h at room temperature. Subsequently, for dehydration, the samples were immersed in 30%, 50%, 70%, and 90% ethanol solutions for 10 min each. Finally, the samples were completely dehydrated by immersing them twice in 100% ethanol for 15 min each. After drying, the platelets that had adhered to the surface of the sample were observed using FE-SEM.

2.7 Evaluation of the IS adsorption performance of the EVOH/AST-120 nanofibers in PBS

An IS solution of 5 mg dL^{-1} was prepared by dissolving IS in PBS. Three milliliters of the IS solution was mixed with the AST-120 powder or EVOH/AST-120 nanofibers and shaken at 37 °C for 8 h using a constant-temperature shaker. At each elapsed time point, the supernatant was collected and colored using an IS measurement kit; then, the IS concentration was calculated by measuring the absorbance of the supernatant using a microplate reader (Tecan Infinite M Nano+). The adsorption capacity of the EVOH/AST-120 nanofibers for IS was calculated by comparing the IS concentration after the adsorption test with its initial concentration.

2.8 Evaluation of the IS adsorption performance of the EVOH/AST-120 nanofibers under blood circulation

Potassium indoxyl sulfate (5.89 mg) was dissolved in 100 mL of porcine blood, to achieve a blood IS concentration of 5 mg dL^{-1}. The EVOH25/AST-120 nanofibers were set in a homemade filter holder in a tubular form, and 30 mL of blood was circulated using a diaphragm pump. At each elapsed time point, blood was collected, and the IS concentration was measured.

The blood samples that were collected at each elapsed time were centrifuged, to separate the plasma, and the hemolysis ratio was assessed by measuring the absorbance of the plasma. The absorbance recorded after the addition of PBS to the blood was set as the 0% hemolysis rate, and the absorbance recorded after the addition of distilled water and all the blood was hemolyzed was set as the 100% hemolysis ratio.

3 Results & discussion

3.1 Fabrication of the EVOH/AST-120 nanofibers

After fabrication *via* electrospinning, the EVOH/AST-120 nanofibers were observed using FE-SEM (Fig. 1). In nanofibers containing EVOH25 (Fig. 1a–d) as well as in nanofibers containing EVOH44 (Fig. 1e–h), the formation of nanofibers with a uniform structure was observed when the AST-120 content was <30 wt%. Of note, the maximum AST-120 content was 30 wt% because spinning was not possible for any of the nanofibers when the AST-120 content was 40 wt%, as the needles became clogged. It is thought that AST-120 was present in the bulges observed in the nanofibers.

The measured fiber diameter distribution of EVOH25/AST-120 nanofibers and EVOH44/AST-120 nanofibers with 30 wt% of AST-120 are depicted in Fig. 1i and j respectively. The mean values of the diameter of each nanofiber were 680 nm and 390 nm. Histograms of fiber diameters, mean, maximum, and minimum values for all nanofibers are shown in Fig. S1 and Table S1.† The fiber diameter decreased with the AST-120 content compared with the pure EVOH nanofibers, and the same phenomenon was observed for both EVOH25 and EVOH44 nanofibers. This could be because the diameter of AST-120 is larger than that of the fiber system; therefore, more EVOH was used to cover the AST-120 surface, thus reducing the amount of EVOH employed to form the nanofibers.

3.2 Confirmation of AST-120 encapsulation using EDX

The elemental mapping of the AST-120 powder and EVOH/AST-120 nanofiber surface by EDX is provided in Fig. 2. On the surface of the activated carbon AST-120 powder (Fig. 2a), X-ray energy derived from the carbon atoms was strongly detected (Fig. 2b), whereas X-ray energy derived from the oxygen atoms was hardly detected (Fig. 2c). This was because AST-120 is a type of activated carbon and is mostly composed of carbon atoms. However, the bulge observed in the center of the EVOH/AST-120 nanofibers (Fig. 2d), which appeared to be AST-120, exhibited strong X-ray energy derived from both carbon and oxygen atoms (Fig. 2e and f). This suggests that EVOH-derived oxygen atoms were detected. Therefore, it was confirmed that AST-120 was fixed in the nanofibers by covering their surface with EVOH. This was thought to be because the AST-120 powder was dispersed in the EVOH solution during the fabrication of the nanofibers using electrospinning, and only the EVOH component remained on the AST-120 surface because of the volatilization of the solvent during electrospinning. The EVOH coating on the surface of AST-120 was expected to prevent the outflow of AST-120 when used in blood, and reduce hemotoxicity by preventing direct contact between AST-120 and blood.

3.3 Characterization of the EVOH/AST-120 nanofibers

Fig. 3a depicts the weight changes of the AST-120 powder, EVOH nanofibers, and EVOH/AST-120 nanofibers during a thermogravimetry-differential thermal analysis (TG-DTA). The weight changes with DTA data are also shown in Fig. S2.† AST-120 has very high thermal stability; therefore, even after a temperature increase to 550 °C, almost no weight change was observed, with a residual mass of 97.8%. On the other hand, EVOH nanofibers and EVOH/AST-120 nanofibers showed 2 steps of weight loss. The first weight loss observed at a temperature below 200 °C is considered due to the evaporation of water inside the materials. The second weight loss was observed from 300 °C to around 450 °C. These temperatures are consistent with the thermal decomposition temperature of EVOH, suggesting that the thermal decomposition of EVOH caused this second weight loss. The DTA curves of these nanofibers in Fig. S2† show the endothermic peaks at these temperatures. These results also suggest that the weight loss of EVOH nanofibers and EVOH/

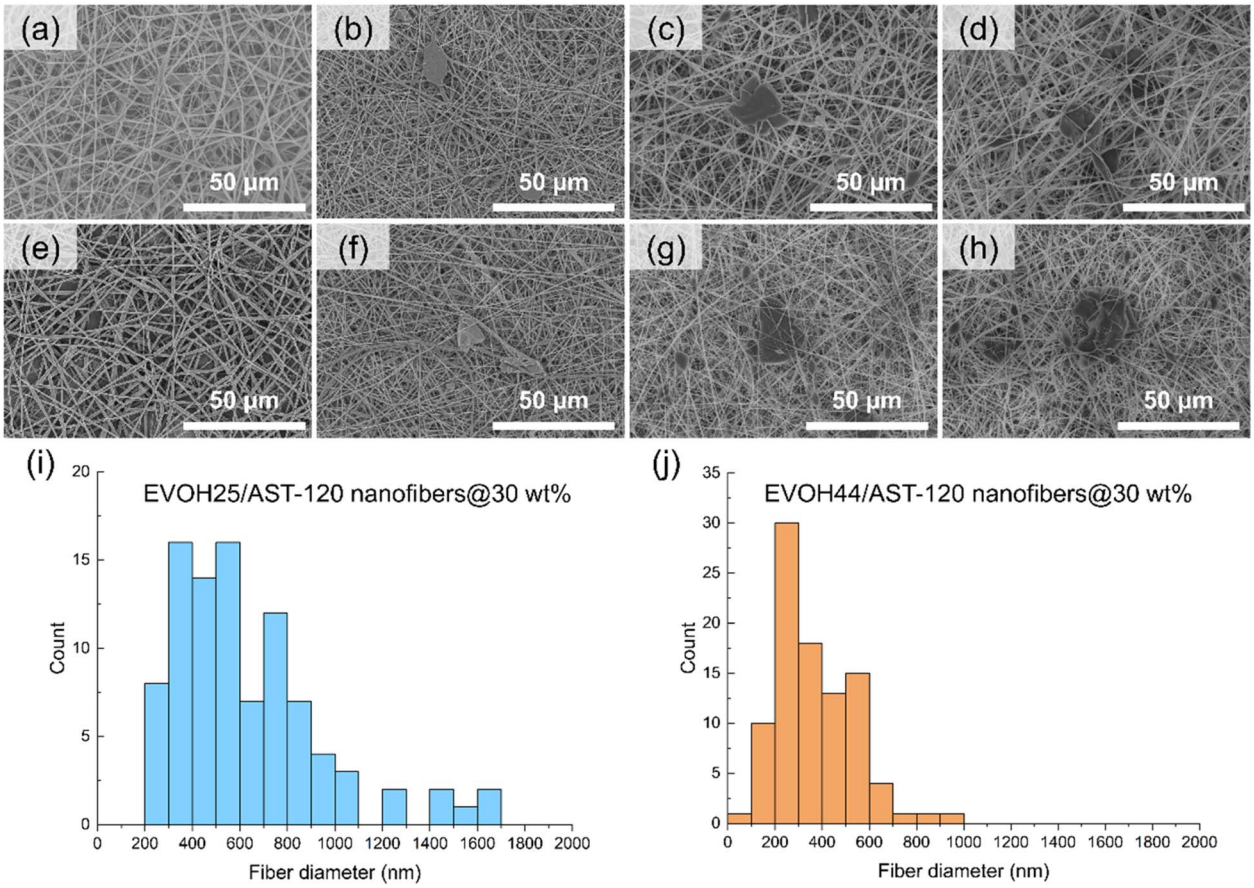

Fig. 1 (a–h): FE-SEM images of the EVOH nanofibers and EVOH/AST-120 nanofibers. The ethylene ratio of EVOH was (a–d) 25 mol% and (e–h) 44 mol%. The content ratio of AST-120 used in the preparation was (a and e) 0 wt%, (b and f) 10 wt%, (c and g) 20 wt%, and (d and h) 30 wt%. (i and j): histogram of fiber diamter of EVOH25/AST-120 and EVOH44/AST-120 nanofibers respectively ($n = 60$). The content ratio of AST-120 was 30 wt%.

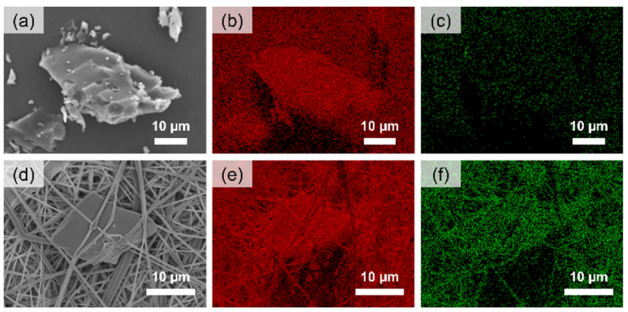

Fig. 2 Elemental mapping image of the AST-120 powder (a–c) and EVOH/AST-120 nanofibers (d–f). The red dots indicate the EDX peak of carbon (b and e) and the green dots indicate the EDX peak of oxygen (c and f).

AST-120 nanofibers are due to water evaporation and thermal decomposition. EVOH nanofibers without AST-120 exhibited residual masses of 2.0% and 2.4% for EVOH25 and EVOH44, respectively. In the case of the EVOH/AST-120 nanofibers, the residual mass was 31.7% and 28.3% for EVOH25/AST-120 and EVOH44/AST-120, respectively. Considering that EVOH hardly remained because of thermal decomposition, the residual of EVOH/AST-120 was considered to be mostly AST-120. Therefore, it was confirmed that AST-120 was contained in the nanofibers in approximately as-prepared quantities.

The results of the analysis of the surface wettability of the EVOH/AST-120 nanofibers using contact angle measurements are reported in Fig. 3b. The increase in the ethylene ratio of EVOH from 25 to 44 mol% increased the contact angle of both the EVOH and the EVOH/AST-120 nanofibers, indicating that their surfaces are more hydrophobic. This may be attributed to an increase in the proportion of ethylene units, which are more hydrophobic, and a decrease in the proportion of vinyl alcohol units, which are more hydrophilic. The surface wettability of the EVOH/AST-120 nanofibers was expected to affect various physical properties, such as the adsorption performance of IS and blood compatibility.

The stress–strain curves of the mechanical strength of the nanofibers, as evaluated using tensile testing, are depicted in Fig. 3c. For both EVOH and EVOH/AST-120, nanofibers with an ethylene ratio of 44 mol% exhibited a higher stress and strain than did those with a ratio of 25 mol%. Previous studies have also reported higher mechanical strength for polyethylene nanofibers compared with polyvinyl alcohol (PVA) nanofibers. For example, the maximum tensile stress of PVA nanofibers, the mechanical

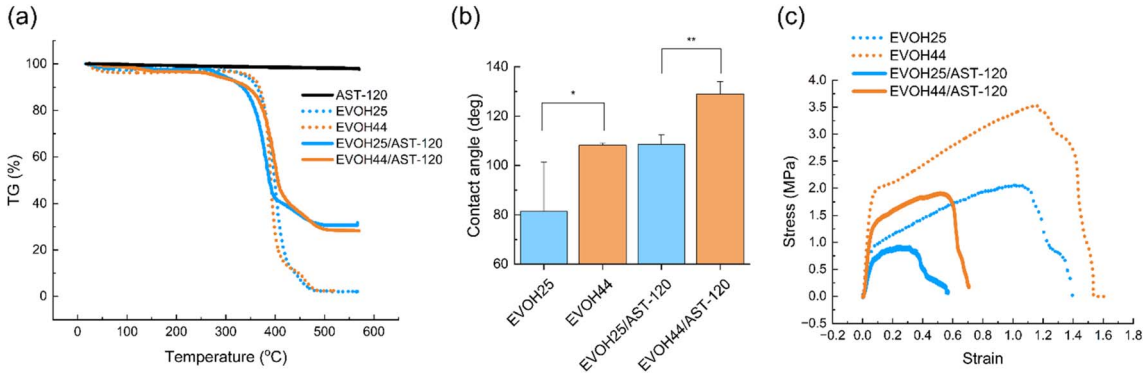

Fig. 3 (a) TG-DTA curve of the AST-120 powder, EVOH nanofibers, and EVOH/AST-120 nanofibers. (b) Water contact angles on the surface of the EVOH nanofibers and EVOH/AST-120 nanofibers. (Mean ± SD, $n = 3$, *$p < 0.05$, **$p < 0.01$). (c) Stress–strain curves of EVOH nanofibers and EVOH/AST-120 nanofibers.

strength of which was improved *via* the solvent volatilization method, is 11.4 MPa,[26] whereas the maximum tensile stress of polyethylene nanofibers reaches 4.9 GPa.[27] Polyethylene has more linear chains than does PVA, which may be explain its higher mechanical strength, as well as its more tightly entangled polymer chains and higher crystallinity. Therefore, it can be inferred that the higher ethylene ratio observed in this nanofiber also improves the mechanical strength because of the dominance of the polyethylene-derived properties.

FT-IR spectra of AST-120 powder, EVOH nanofibers, and EVOH/AST-120 nanofibers are shown in Fig. S3.† Several absorbance peaks derived from EVOH were observed in at 2853 cm^{-1} (C–H), 2926 cm^{-1} (C–H) and around 3300 cm^{-1} (O–H), which can be related to stretching vibrations, and at 1329 cm^{-1} (C–H) and 1456 cm^{-1} (C–H) due to bending vibrations in the spectra of EVOH nanofibers and EVOH/AST-120 nanofibers.[28] The absorbance peak derived from AST-120 was also observed at 2317 cm-1 (C═C) in AST-120 and EVOG-AST-120 nanofibers.[29] In addition, numerous noisy peaks were observed in AST-120 and EVOH/AST-120 at 3500 to 4000 cm^{-1} and 1300 to 1700 cm^{-1}, which appeared to originate from the surface functional groups of AST-120. Absorption peaks at the same wavenumber were observed for AST-120 powder and EVOH/AST-120 nanofibers. These results also confirmed the presence of EVOH and AST-120 in the EVOH/AST-120 nanofibers. The peak observed around 3300 cm^{-1} in the nanofibers was considered to be derived from hydroxy groups, but its peak position showed different values for different nanofibers. The peak position was 3316 cm^{-1} for EVOH25 and EVOH44, 3289 cm^{-1} for EVOH25/AST-120, and 3300 cm^{-1} for EVOH44/AST-120. EVOH25/AST-120 showed the peak shift to the lowest wavenumber among these samples. This may be due to the increased amount of hydroxy groups in the sample with EVOH25, which resulted in stronger hydrogen bonding, which suppressed molecular vibrations.[30]

3.4 Evaluation of the adsorption performance of the EVOH/AST-120 nanofibers for IS

The IS adsorption performance of the EVOH/AST-120 nanofibers immersed in the IS solution was evaluated. Fig. 4 reports

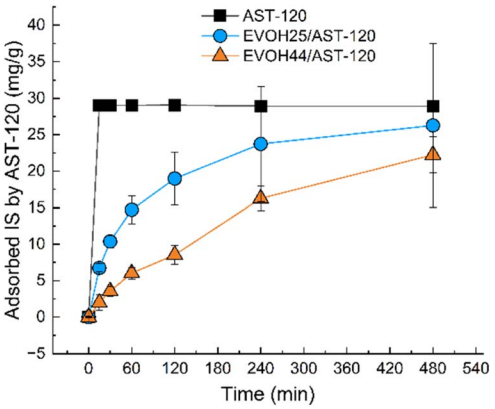

Fig. 4 IS adsorption capacity of AST-120 in the powder state (black line) and in EVOH/AST-120 nanofibers (blue and orange line). (Mean ± SD, $n = 3$).

the change in IS adsorption over time per mass of AST-120 in the powdered or nanofiber state. We confirmed that the IS adsorption rate decreased when AST-120 was included in the nanofibers compared with its powder state. To achieve IS adsorption onto AST-120 in the EVOH/AST-120 nanofibers, it must diffuse between the polymer chains of EVOH covering the AST-120 surface and reach AST-120. Because this diffusion process takes time, the adsorption rate is thought to have decreased. In this case, EVOH25/AST-120 showed a higher adsorption rate compared with EVOH44/AST-120. As shown in Fig. 3b, EVOH25/AST-120 was more hydrophilic, which may be attributed to its higher diffusion rate. Because the treatment time of hemodialysis is approximately 4 h, the column should show a high adsorption capacity within 4 h when used as an IS-adsorbing column. Fig. 4 reveals that the IS-adsorption capacity of EVOH25/AST-120 reached a value that was not significantly different from that of the AST-120 powder after 4 h, indicating that it is useful for treatment. This final IS-adsorption capacity of AST-120 in EVOH25/AST-120 was 26.3 mg g^{-1}, a 68-fold improvement in adsorption performance over EVOH/zeolite nanofibers within our previous study.[15] The improved adsorption capacity is expected to significantly reduce the amount of

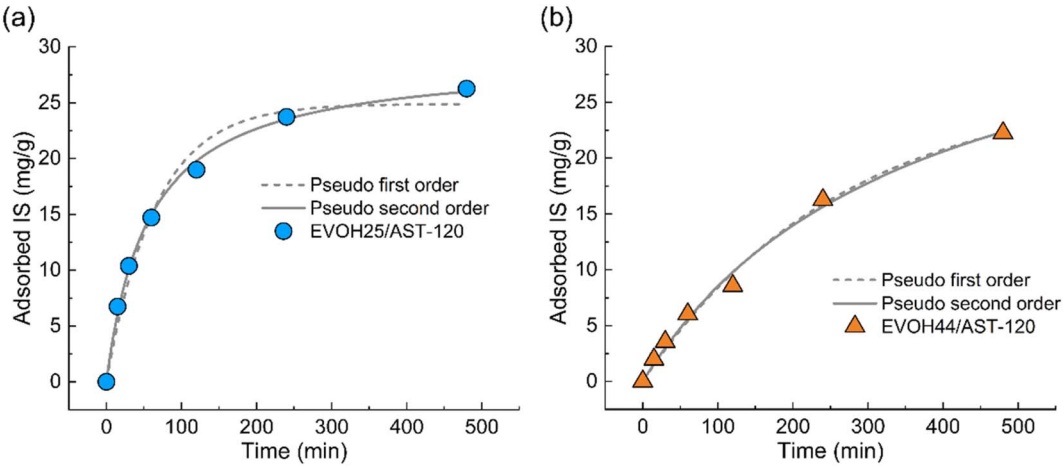

Fig. 5 Pseudo-first-order model and pseudo-second-order model of IS adsorption by (a) EVOH25/AST-120 nanofibers and (b) EVOH44/AST-120 nanofibers.

Table 1 Comparison of the pseudo-first-order and pseudo-second-order model kinetics of the EVOH/AST-120 nanofibers

	Fitting model	Q_e (mg g^{-1})	k_1 (min^{-1})	k_2 (g mg^{-1} min^{-1})	R^2
EVOH25/AST-120	Pseudo-first-order	24.89	0.015	—	0.9769
	Pseudo-second-order	29.04	—	6.110×10^{-4}	0.9971
EVOH44/AST-120	Pseudo-first-order	26.55	0.004	—	0.9919
	Pseudo-second-order	39.08	—	7.123×10^{-5}	0.9922

nanofibers required for treatment, which is a significant step forward toward practical application.

The kinetics of the adsorption of IS by the EVOH/AST-120 nanofibers were analyzed using a pseudo-first-order and a pseudo-second-order model,[31] and the results are reported in Fig. 5 and Table 1. These parameters were calculated using eqn (1) and (2), respectively:

$$Q_t = Q_e(1 - e^{-k_1 t}) \quad (1)$$

$$Q_t = \frac{k_2 Q_e^2 t}{1 + k_2 Q_e t} \quad (2)$$

where t is the elapsed time, Q_e is the maximum adsorption capacity, Q_t is the adsorption capacity at each time point, and k_1 and k_2 are the rate constants. EVOH25/AST-120 exhibited higher rate constants in both the pseudo-first-order and pseudo-second-order models. Regarding the R^2 values, both EVOH25/AST-120 and EVOH44/AST-120 were better fitted by the pseudo-second-order model than they were by the pseudo-first-order model. Accordingly, in recent years, many diffusion-based adsorption processes have been reported to be represented by pseudo-second-order model.[32,33] Therefore, this result suggests that the diffusion of IS molecules between the polymer chains of EVOH covering the AST-120 surface is the rate-limiting step, as described above, and that the difference in hydrophobicity caused by the ethylene ratio of EVOH plays a major role in this process.

3.5 Hemocompatibility of the EVOH/AST-120 nanofibers

Because albumin is an essential protein for living organisms, its adsorption by nanofibers must be suppressed. Fig. 6a shows the adsorption of human serum albumin (HSA) by the AST-120 powder and each of the nanofibers. There was no significant difference between the nanofibers, in turn, the amount of HSA adsorbed by each type of nanofiber was significantly lower than that observed for the AST-120 powder. When the AST-120 powder was in direct contact with blood, HSA was adsorbed by activated carbon. In contrast, the surface of the EVOH/AST-120 nanofibers is covered by the EVOH component; thus, AST-120 was not in direct contact with blood. This was thought to have inhibited the adsorption of HSA.

In addition, platelet adhesion must also be inhibited because platelets, which are a component of the blood, cause blood coagulation when they adhere and aggregate on the surface of the material. After the immersion of each nanofiber in PRP, the adhered platelets were fixed and counted based on the SEM images, as depicted in Fig. 6b. For both the EVOH and EVOH/AST-120 nanofibers, platelet adhesion was higher in nanofibers with an ethylene ratio of 25 mol%. A previous study that investigated the relationship between the contact angle and platelet adhesion reported that a higher water contact angle at the material surface was associated with a higher platelet adhesion rate.[34] In the EVOH/AST-120 nanofibers, a larger water contact angle was observed for an ethylene ratio of 25 mol%. An enhanced interaction with platelets may have resulted in increased platelet adhesion. After their activation, adherent platelets elongate pseudopodia and form aggregates, thus leading to blood coagulation.[35,36] In Fig. 6c, which depicts platelets adhering onto EVOH25/AST-120, the platelets maintained a spherical shape and did not appear to be activated. Therefore, platelet adhesion did not appear to cause serious hemotoxicity.

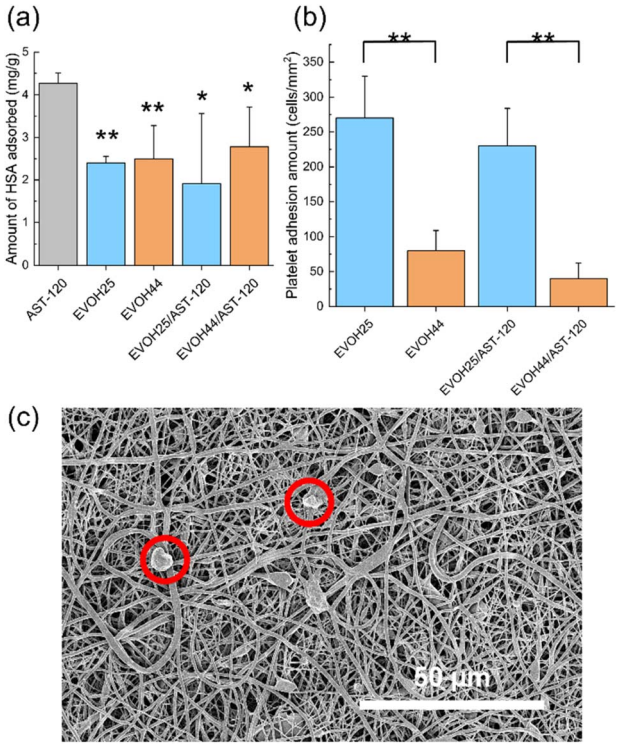

Fig. 6 (a) Amount of human serum albumin adsorbed by the AST-120 powder and nanofibers. (Mean ± SD, $n = 3$, *$p < 0.05$, **$p < 0.01$). (b) Amount of platelet adhesion to nanofibers, as assessed based on the FE-SEM image. (Mean ± SD, $n = 10$, **$p < 0.01$). (c) FE-SEM image of platelets adhering onto the EVOH25/AST-120 nanofibers.

3.6 IS adsorption test under blood circulation conditions

An experiment was conducted using EVOH25/AST-120 to determine if IS could be adsorbed under blood circulation conditions. Fig. 7 report the changes in the IS concentration and hemolysis ratio over time in the blood after 4 h of circulation of nanofibers placed in a homemade filter holder in porcine blood. The IS concentration in the blood decreased from an initial concentration of 5.04 mg dL^{-1} to 3.54 mg dL^{-1}. This finding suggests that IS can be adsorbed even when it is bound to albumin in the blood. Although the IS concentration could not be reduced below the standard value of 50 μg dL^{-1}, the nanofibers are intended to be used in combination with hemodialysis as an adsorption column for IS. Considering that, to some extent, IS can be removed by hemodialysis, the amount of IS removed in this experiment is considered to be sufficient.

The hemolysis ratio of porcine blood increased with time, reaching 9.88% after 4 h. It has been reported that a hemolysis ratio of 10% does not indicate serious toxicity;[37] here, we were able to maintain the hemolytic rate below this threshold.

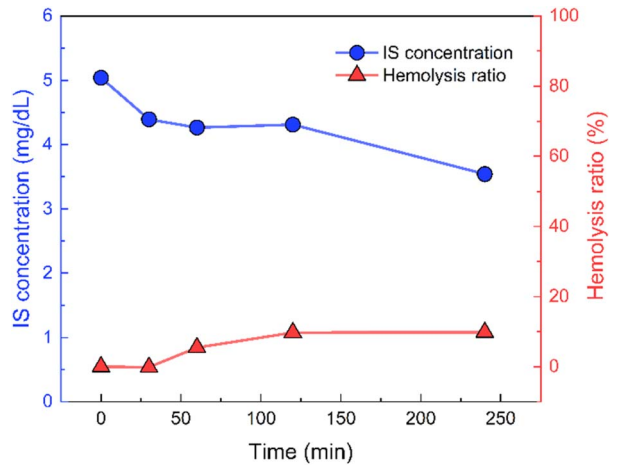

Fig. 7 IS concentration (blue line) and hemolysis ratio (red line) recorded during the blood circulation test.

4 Conclusions

EVOH/AST-120 nanofibers were prepared using electrospinning for the adsorption of IS in the blood using two types of EVOH (with ethylene ratios of 25 mol% and 44 mol%, respectively), both with a maximum AST-120 content of 30 wt%. The EVOH25/AST-120 nanofibers exhibited a higher IS adsorption rate than did their EVOH44/AST-120 counterparts, which was attributed to its greater surface hydrophilicity, as suggested by contact angle measurements. Furthermore, the adsorption behaviors fit well with the pseudo-second-order model, indicating that diffusion was the rate-limiting step for IS adsorption. The difference in the diffusion rate of IS observed between the nanofibers may have affected its adsorption rate. Moreover, hemocompatibility studies showed that the amount of HSA adsorption was reduced by the inclusion of AST-120 in the nanofibers. Platelet adsorption was higher for EVOH25/AST-120 nanofibers, possibly because of the hydrophilic nature of their surface. Finally, the IS adsorption performance was examined under the following blood circulation conditions, and the IS concentration in the blood was successfully reduced to 70.3% of the initial level. The use of this nanofiber in combination with hemodialysis as an IS adsorption filter is expected to provide sufficient therapeutic effects.

Data availability

Raw data were generated at National Institute for Materials Science, Japan. Derived data supporting the findings of this study are available from the corresponding author on request.

Author contributions

Makoto Sasaki: conceptualization, methodology, investigation, writing – original draft, visualization. Rieko Hirata: conceptualization, resources, writing – review & editing. Ayano Konagai: resources, writing – review & editing, supervision. Mitsuhiro Ebara: conceptualization, writing – review & editing, supervision, project administration, funding acquisition.

Conflicts of interest

There are no conflicts to declare.

Acknowledgements

This work was supported by JSPS KAKENHI Grant Number JP20H05877 and JP23KJ0260. A part of this work was supported by "Advanced Research Infrastructure for Materials and Nanotechnology in Japan (ARIM)" of the Ministry of Education, Culture, Sports, Science and Technology (MEXT).

References

1 R. Vanholder, R. De Smet, G. Glorieux, A. Argilés, U. Baurmeister, P. Brunet, W. Clark, G. Cohen, P. P. De Deyn, R. Deppisch, B. Descamps-Latscha, T. Henle, A. Jörres, H. D. Lemke, Z. A. Massy, J. Passlick-Deetjen, M. Rodriguez, B. Stegmayr, P. Stenvinkel, C. Tetta, C. Wanner and W. Zidek, *Kidney Int.*, 2003, **63**, 1934–1943.
2 K. Sakai, *J. Membr. Sci.*, 1994, **96**, 91–130.
3 Y. Motomiya, Y. Ando, K. Haraoka, X. Sun, H. Iwamoto, T. Uchimura and I. Maruyama, *Kidney Int.*, 2003, **64**, 2244–2252.
4 B. K. I. Meijers, H. De Loor, B. Bammens, K. Verbeke, Y. Vanrenterghem and P. Evenepoel, *Clin. J. Am. Soc. Nephrol.*, 2009, **4**, 1932–1938.
5 H. Hou, M. Horikawa, Y. Narita, H. Jono, Y. Kakizoe, Y. Izumi, T. Kuwabara, M. Mukoyama and H. Saito, *Int. J. Mol. Sci.*, 2023, **24**, 1–14.
6 T. Niwa, *Nagoya J. Med. Sci.*, 2010, **72**, 1–11.
7 H. Fujii, K. Nakai and M. Fukagawa, *Ther. Apher. Dial.*, 2011, **15**, 125–128.
8 S. C. Hung, K. L. Kuo, C. C. Wu and D. C. Tarng, *J. Am. Heart Assoc.*, 2017, **6**, 1–8.
9 S. C. Leong and T. L. Sirich, *J. Toxins*, 2016, **8**, 358–370.
10 M. Asai, S. Kumakura and M. Kikuchi, *Ren. Fail.*, 2019, **41**, 47–56.
11 G. Schulman, T. Berl, G. J. Beck, G. Remuzzi, E. Ritz, K. Arita, A. Kato and M. Shimizu, *J. Am. Soc. Nephrol.*, 2015, **26**, 1732–1746.
12 W. C. Liu, Y. Tomino and K. C. Lu, *J. Toxins*, 2018, **10**, 1–22.
13 K. Namekawa, M. Tokoro Schreiber, T. Aoyagi and M. Ebara, *Biomater. Sci.*, 2014, **2**, 674–679.
14 R. Takai, R. Kurimoto, Y. Nakagawa, Y. Kotsuchibashi, K. Namekawa and M. Ebara, *J. Nanomater.*, 2016, **2016**, 1–7.
15 M. Sasaki, Y. Liu and M. Ebara, *Fibers*, 2021, **9**, 1–11.
16 N. Bhardwaj and S. C. Kundu, *Biotechnol. Adv.*, 2010, **28**, 325–347.
17 C. Bavatharani, E. Muthusankar, S. M. Wabaidur, Z. A. Alothman, K. M. Alsheetan, M. mana AL-Anazy and D. Ragupathy, *Synth. Met.*, 2021, **271**, 116609.
18 T. Mukhiya, A. Muthurasu, A. P. Tiwari, K. Chhetri, S. H. Chae, H. Kim, B. Dahal, B. M. Lee and H. Y. Kim, *ACS Appl. Mater. Interfaces*, 2021, **13**, 23732–23742.
19 N. G. Siddamallappa, M. Basavaraju and C. G. Dase Gowda, *Polym. Int.*, 2018, **67**, 1511–1522.
20 B. Mahesh, D. Kathyayani, G. S. Nanjundaswamy, D. Channe Gowda and R. Sridhar, *Carbohydr. Polym.*, 2019, **212**, 129–141.
21 B. Mahesh, D. Kathyayani, D. Channe Gowda, A. Sionkowska and S. Ramakrishna, *Mater. Chem. Phys.*, 2022, **281**, 125847.
22 G. S. Nanjundaswamy, B. Mahesh, G. D. Channe, N. A. Chamaraja and G. Angadi, *Polym. Technol. Mater.*, 2021, **60**, 405–418.
23 H. Matsuyama, K. Kobayashi, T. Maki, M. Tearamoto and H. Tsuruta, *J. Appl. Polym. Sci.*, 2001, **82**, 2583–2589.
24 T. Huang, J. Song, L. Xing, X. Li and T. He, *J. Membr. Sci.*, 2019, **579**, 172–179.
25 Y. Ishii, S. Yarn, H. Kanai, A. Maezawa, A. Tsuchida, R. Wakamatsu and T. Naruse, *Nephron*, 1996, **73**, 407–412.
26 A. Rianjanu, A. Kusumaatmaja, E. A. Suyono and K. Triyana, *Heliyon*, 2018, **4**, e00592.
27 J. H. Park and G. C. Rutledge, *J. Mater. Sci.*, 2018, **53**, 3049–3063.
28 A. Aragón-Gutiérrez, R. Heras-Mozos, M. Gallur, D. López and P. Hernández-Muñoz, *Foods*, 2021, **10**, 1–18.
29 N. Mojoudi, N. Mirghaffari, M. Soleimani, H. Shariatmadari, C. Belver and J. Bedia, *Sci. Rep.*, 2019, **9**, 1–12.
30 K. Uto, Y. Liu, M. Mu, R. Yamamoto, C. Azechi, M. Tenjimbayashi, A. Kaeser, M. A. Marliac, M. M. Alam, J. Sasai and M. Ebara, *Adv. Mater. Interfaces*, 2024, **11**, 1–10.
31 Y. S. Ho and G. Mckay, *Process Biochem.*, 1999, **34**, 451–465.
32 M. A. Hubbe, S. Azizian and S. Douven, *BioResources*, 2019, **14**, 7582–7626.
33 T. Hoshi, M. Endo, A. Hirai, M. Suzuki and T. Aoyagi, *Pharmaceutics*, 2020, **12**, 1–16.
34 J. H. Lee and H. B. Lee, *J. Biomed. Mater. Res.*, 1998, **41**, 304–311.
35 A. C. Swanepoel and E. Pretorius, *Hematology*, 2015, **20**, 39–47.
36 J. Y. Park, C. H. Gemmell and J. E. Davies, *Biomaterials*, 2001, **22**, 2671–2682.
37 K. Amin and R. Dannenfelser, *J. Pharm. Sci.*, 2006, **95**, 1173–1176.